Original

Ivanou, D.; Yasakau, K.; Kallip, S.; Lisenkov, A.; Starykevich, M.; Lamaka, S.; Ferreira, M.; Zheludkevich, M.:

Active corrosion protection coating for ZE41 magnesium alloy created by combining PEO and sol-gel techniques

In: RSC Advances (2016) Royal Society of Chemistry

DOI: 10.1039/C5RA22639B

RSC Advances

PAPER

View Article Online
View Journal | View Issue

Cite this: *RSC Adv.*, 2016, **6**, 12553

Active corrosion protection coating for a ZE41 magnesium alloy created by combining PEO and sol–gel techniques

D. K. Ivanou,*[a] K. A. Yasakau,[b] S. Kallip,[b] A. D. Lisenkov,[b] M. Starykevich,[b] S. V. Lamaka,[cd] M. G. S. Ferreira[b] and M. L. Zheludkevich[bd]

Received 28th October 2015
Accepted 22nd January 2016

DOI: 10.1039/c5ra22639b

www.rsc.org/advances

An active protective coating for ZE41 magnesium alloy was produced by sealing an anodic layer, loaded with 1,2,4-triazole, with a sol–gel film. An anodic oxide layer was formed using PEO in a silicate–fluoride alkaline solution. This thin (1.8 μm) porous PEO layer was impregnated with corrosion inhibitor 1,2,4-triazole and sealed with a silica-based sol–gel film modified with titanium oxide. For the first time it was demonstrated that this relatively thin PEO-based composite coating revealed high barrier properties and provided superior protection against corrosion attack during 1 month of continuous exposure to 3% NaCl. A scanning vibrating electrode technique showed a sharp decrease (100 times) of corrosion activity in micro defects formed in the 1,2,4-triazole doped composite coating, when compared to blank samples.

1. Introduction

Magnesium made components are integral parts of much military, electronic and medical equipment. However, the obstacle for wide use of magnesium alloys is the high chemical activity and corrodibility of Mg.[1,2] Outstanding surface processing is required to minimize its suffering from corrosion. There are a variety of physical, chemical and electrochemical treatments like deposition from gas-phase, laser assisted melting, chemical conversion, coating with organic films, electroless deposition, electroplating,[3–7] and anodizing yielding barrier-type films, all providing good corrosion protection.[8–11] During the two last decades, plasma electrolytic oxidation (PEO) of magnesium alloys became widely used.[12–22] Keronite,[18,19] Tagnite,[20] Magoxid[21] and Anomag[22] are among the most commonly, commercially used PEO techniques for magnesium alloys.

Formed by PEO anodic films possess high adhesion and hardness. Dense and porous layers could be clearly recognized in the coatings. The outer porous layer could not protect Mg from corrosion and the appearance of microdefects in the dense layer significantly reduces the positive effect from PEO treatment. Current studies on anodizing range from coating formation to post-treatment techniques.[6,23–33] Sol–gel treatment[23–27] and organic film coating,[28,29] hardening with alkaline solutions of silicates and phosphates,[25] electroless metal deposition,[30,31] E-coating,[32] *in situ* sealing[33] are utilized to increase protective performance of PEO coatings.

State of the art sol–gel formulations allow production of the robust composite primer for Mg alloys that provides both good adhesion of the organic paint and corrosion protection.[6,34–39] Addition of corrosion inhibitors to coatings imparts them with the important property of active protection and improve overall protective performance, providing that the coating's barrier properties are not affected by, often detrimental, chemical interaction of inhibitors with components of the coatings.[6,24,40,41]

A composite coating is a necessity when long lasting durable protection needs to be provided to one of the most corrosion susceptible Mg alloys, such as ZE41, used in this work.[42] This article presents a novel coating for magnesium alloy with active protection against corrosion attack.

Traditionally it is considered that PEO coating should be relatively thick (tens μm) to provide a good protection against corrosion attack. In the present work we report that even thin PEO coatings (1.8 μm) formed in soft "spark" anodizing regime, combined with appropriate inhibitor and sealant is sufficient for providing lasting active protection to Mg alloy. The coating consists of a porous PEO formed oxide layer loaded with corrosion inhibitor, 1,2,4-triazole,[43,44] and a layer of sol–gel sealant. Anodic film serves as an additional intermediate barrier between the Mg alloy and the sol–gel sealant. Thin porous PEO layer is enriched with the corrosion inhibitor. It

[a]*LEPABE, Faculty of Engineering, University of Porto, 4200-465 Porto, Portugal. E-mail: Ivanovdk@gmail.com; Tel: +351-920-427-795*

[b]*Department of Materials and Ceramic Engineering, CICECO-Aveiro Institute of Materials, University of Aveiro, 3810-193 Aveiro, Portugal*

[c]*Centro de Quimica Estrutural, Instituto Superior Técnico, Universidade de Lisboa, Av. Rovisco Pais, 1049-001 Lisboa, Portugal*

[d]*MagIC – Magnesium Innovation Centre, Institute of Materials Research, Helmholtz-Zentrum Geesthacht, 21502 Geesthacht, Germany*

further improves corrosion protection of the coating as a whole and imparts important element of active corrosion protection.

In this work the sol–gel coating with very robust barrier at relatively low thickness was employed. Our novel sol–gel was prepared with reduced quantity of harmful volatile solvents or diluents, as opposed to common sol–gel preparation routes that use alcohols as solvents.[34] This work demonstrates good corrosion protection of duplex PEO/sol–gel coating and the ability of 1,2,4-triazole loaded into the anodic oxide to delay the corrosion attack after the coating is intentionally damaged.

2. Experimental section

2.1. Reagents and materials

As metallic substrates coupons of extruded commercial ZE41 magnesium alloy (3.5–5.0 wt% Zn, 0.4–1.0 wt% Zr, 0.75–1.75 wt% Ce and Mg balance) were used. The coupons were cut to 40 mm × 25 mm × 2 mm in size and abraded with emery paper 600, 800 and 1200 grits (Struers, SiC). Absolute ethanol was used as an antifriction medium at the last stage of abrading. The plates were rinsed with ethanol and dried. Sigma-Aldrich high purity grade reagents were used in this work. MilliPore purified water (ρ > 18 MΩ cm) was used for solutions.

2.2. Plasma electrolytic oxidation and inhibitor impregnation

The details of the PEO process used in this work were similar to those explained in our recent publication.[27] 16 wt% HF aqueous solution was used for etching cleaned ZE41 samples at 20 ± 2 °C during 15–20 min before anodizing. HF-treated substrates were washed with distilled water and dried in a flow of compressed air. As the DC source in all anodization experiments an Agilent® N5751A DC power supply (300 V, 2.5 A, 750 W) was used. The sample served as the anode and a stainless steel cup (200 mL) was used as the cathode. Anodization was performed in electrolyte consisting of 16 g L^{-1} Na_2SiO_3, 10 g L^{-1} KF, 6 g L^{-1} NaOH and 7.5 g L^{-1} poly(ethylene oxide), MW ~ 600.000. Metal plates were anodized at 3 mA cm^{-2} for 12 min at 20 ± 2 °C in stirred electrolyte. The samples were then washed at room temperature with distilled water and dried in compressed air flow.

The resulting porous oxide was impregnated with inhibitor by immersing the plates of anodized magnesium in 0.01 M aqueous solution of 1,2,4-triazole for 15 s with drying in compressed air flow.

2.3. Sol–gel coatings preparation and application

Controlled hydrolysis of organosiloxanes 3-glycidoxypropyltrimethoxysilane (GPTMS), titanium(IV) propoxide (TPOT) and phenyltrimethoxisilane (PTMS) precursors and aqueous acid solution was used for preparation of hybrid sols. The sol–gel preparation procedure was similar to that used in ref. 45 while a new component, PTMS, was added along with GPTMS. The coating formulation was prepared by dissolving separately a silane sol (composed of GPTMS + PTMS) and metal organic sol and then mixing both sols to obtain the final sol–gel formulation. The first sol was formed by mixing GPTMS and PTMS (volume ratio was 1 : 1). It was hydrolyzed by 0.316 M HNO_3 acid in a 3 : 1 molar ratio of water to hydrolysable groups under constant stirring for one hour. The second solution was produced by mixing TPOT (70 wt% in 2-propanol) and acetylacetone in stoichiometric proportion for 20 min. Then the solution was hydrolyzed for one hour in the presence of 0.316 M HNO_3. At the final stage, both metal organic and silane based sols were mixed together for one hour followed by ageing for one more hour. During the synthesis steps the solutions were held at a constant temperature of 22 ± 1 °C in a water circulating, thermostat system.

Several types of coated substrates were prepared. ZE41 coupons etched in HF were dipped in the hybrid sol–gel formulation for 40 seconds and withdrawn at a speed of 18 cm min^{-1}. PEO treated ZE41 samples were immersed in the sol–gel for 100 seconds and also withdrawn at a speed of 18 cm min^{-1}. The coated samples were suspended at room temperature (24 ± 2 °C) and relative humidity of around 60% in open air for one hour, then cured at 120 °C for 1.5 h in an oven. Three different types of ZE41 samples were tested: (1) sol–gel coated ZE41, **ZE_SG**; (2) sol–gel sealed PEO treated alloy, **ZE_Anod_SG**; (3) PEO treated ZE41 immersed in solution of 1,2,4-triazole and sealed with a film of sol–gel, **ZE_Anod_Tr_SG**.

2.4. Electrochemical techniques

The EIS study was performed using a Gamry FAS2 Femtostat at 20 ± 1 °C in a pH neutral 3% NaCl solution. The exposed surface area was 3.3 cm^2. The samples were measured in a frequency range of 100 kHz to 10 mHz by applying peak to peak sinusoidal perturbations of 10 mV at open circuit potential. During the measurements per decade of frequency seven experimental points were collected. To check the reproducibility at least three samples were tested for each type of coating. The results differ within 7 ± 2%, the worst results are presented. To avoid any electro–magnetic interference all of the measurements were performed in a Faraday cage. Impedance plots were fitted using Gamry Echem Analyst software, simplex method was employed. The values of the "true" capacitance were calculated from constant phase element (CPE) using the relationship $C = (R \times \mathrm{CPE})^{(1/n)}/R$.

SVET measurements were performed using commercial instrument from Applicable Electronics Inc. (USA) controlled by the ASET 2.0 software from ScienceWares Inc. (USA). Pt–Ir wires (MicroProbes Inc. (USA)) were used as electrodes. The electrodes were with an insulated shaft and a platinum black deposit on the tip up to 10 μm in diameter. The operation conditions of the probe was: 100 μm above the surface; vibration in the normal direction to the surface; amplitude 10 μm; frequency 398 Hz. The calibration included conversion of the measured potential differences in solution, caused by ionic fluxes, into the ionic currents.[46] Ionic currents aroused from electrochemical reactions on the surface of corroding metal.

2.5. Structure characterization

Semi-in-lens Hitachi SU-70 UHR Schottky Analytical FE-SEM coupled with a Bruker EDS detector microscope was used for

characterization of the structure and composition of the obtained PEO films. Cross-section analysis was performed on embedded into epoxy resin samples. The final grit of SiC emery paper used for abrasion was 4000. In order to determine the composition of the anodized layers and sol–gel precise EDS analysis of cross-sectioned samples from a square area $0.9 \times 0.9\ \mu m^2$ positioned in the middle of anodic film and sol–gel was performed.

X-ray diffraction (XRD) studies of the coatings were performed using a Philips X'Pert MPD diffractometer (Bragg–Brentano geometry, Cu Kα radiation).

Glow Discharge Optical Emission Spectroscopy (GDOES) depth profile analysis was performed using a HORIBA GD-Profiler 2 with an anode of 4 mm in diameter. It was operated at a constant power of 30 W in a nitrogen atmosphere of 650 Pa. To obtain depth profiles light emissions of characteristic wavelengths were monitored with 10 ms sampling time. The wavelengths of the spectral lines used for Mg, O, Si, and C were 285.213, 130.217, 288.158 and 165.70 respectively.

3. Results and discussion

3.1. PEO treatment of ZE41

Unlike most of the earlier presented PEO treatments,[12,13,17,28] our method resulted in formation of a thin coating. This is because our main aim was to produce a porous reservoir for corrosion inhibitors rather than a thick protective layer by PEO treatment. The thickness of the PEO layer was (1.8 ± 0.1 μm). The film was amorphous for XRD and according to EDS analysis composed of Mg (24.7 ± 0.8 at%), O (52.4 ± 0.9 at%), Si (12.6 ± 0.7 at%) and F (10.3 ± 0.6 at%). The surface morphology is characterized by irregular round pores of 0.2 to 3 μm that homogeneously cover the surface (Fig. 1a). PEO coating sealed with sol–gel coating was also amorphous for XRD. Sol–gel layer was mainly composed of Ti, Si and O in molar ratio 1 : 5 : 12.

Fig. 1b and c show cross-sectional SEM micrographs coupled with EDS mappings of a **ZE_Anod_Tr_SG** sample. The sol–gel coating uniformly covers the PEO layer and fills its pores without any defects at the interface.

Fig. 1c shows the EDS signal from nitrogen atoms. It is clearly seen that the most intense signal is emanating from the PEO layer. This shows the low release of 1,2,4-triazole into the sealant at the sol–gel application stage. This fact is important because chemical interaction of inhibitor with the components of the sol–gel sealant impairs the polymerization; reduces film homogeneity and active concentration of the inhibitor. Good retention of 1,2,4-triazole in the PEO layer is more likely to be attributed to its porous structure, composed of amorphous magnesium oxide/hydroxide species which possess chemical affinity to triazole.

Additional characterization of PEO films and sol–gel sealed films were performed using the GDOES technique. Fig. 2a depicts GDOES elemental "depth" profiles of an anodized ZE41 sample. Two regions can be clearly identified in the spectra. Region **I** is characterized by relatively strong signals from O and Si atoms and a low signal from Mg. It is observed at sputtering times from 0 to ~70 s and might be associated with the porous layer of the anodic coating. Region **II**, at sputtering times >70 s, with an exponential decrease of the responses from O and Si along with a pronounced signal from Mg, corresponds to the inner, dense layer of the PEO film. At sputtering times >150 s the response from O and Si can barely be detected in the spectra while the Mg emission signal becomes saturated, indicating that the PEO film is completely sputtered. The GDOES profile spectra for **ZE_Anod_Tr_SG** are presented in Fig. 2b.

Between 0 to ~220 s, time-stable signals from O, Si and C are observed pointing to the homogeneous structure of the sol–gel sealant. The response from the sol–gel/PEO film interface

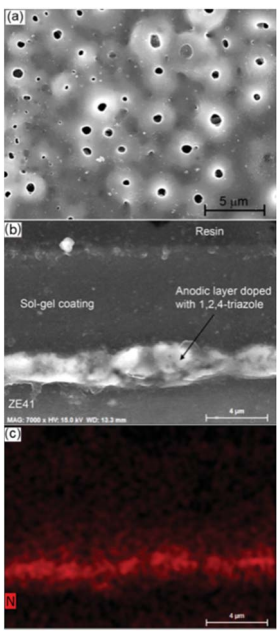

Fig. 1 SEM micrographs of anodized ZE41: (a) plane view, (b) cross-section view of **ZE_Anod** and (c) EDS signal from nitrogen atoms of **ZE_Anod_Tr_SG** samples.

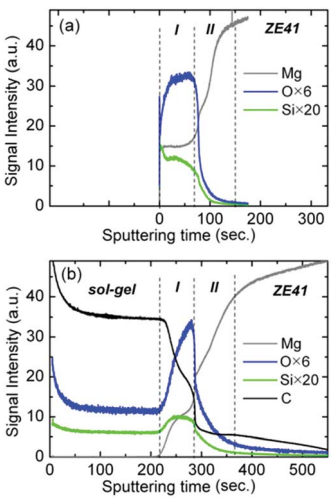

Fig. 2 GDOES element profiles for **ZE_Anod** (a) and **ZE_Anod_Tr_SG** (b) samples. To guide the eyes the plot (a) is positively shifted along "Sputtering time" axis.

manifests itself at ~220 s: the signals from O and Si increase and C signal decrease.

It is noteworthy that the slope of the carbon signal in region **I** is in opposition to the signal from Mg pointing to a uniform sealing of the porous oxide layer with sol–gel.

The level of carbon signal in region **II**, *i.e.* in the inner dense of the anodic coating, in the level of the background signal (the "tail" in the spectra at sputtering times >375 s). This fact points to low concentration of the cracks in the dense PEO layer within the relatively high (4 mm in diameter) sputtering area.

3.2. Protective behavior of sol–gel coating

The sol–gel coating thickness is 6.3 ± 0.2 μm and it evenly covers the surface of the PEO layer, (Fig. 1b). Long term corrosion resistance of the sol–gel coating, directly applied on ZE41, was studied by EIS in a naturally aerated 3% NaCl solution. Fig. 3a depicts Bode plots for a **ZE_SG** sample. At the beginning of the test, the EIS response from **ZE_SG** sample could be adequately simulated by two time constants connected in cascade (Fig. 3b). The resistance of 3% NaCl solution is simulated with R_{sol}. To adjust the phase shift constant phase elements (CPE) were used for fitting the spectra.[47] The resistance R_{SG} and CPE_{SG} simulate the sol–gel coating and R_{in}, CPE_{in} – intermediate species forming in the coating/substrate interface.

On the 3rd day of immersion a new time constant, manifesting itself at about 1 Hz frequency appeared pointing to initiation of the corrosion attack. As a result the double-layer capacitance (CPE_{dl}) and resistance (R_{polar}) should be included into equivalent circuit (Fig. 3c).

Fig. 4 presents the evolution of R_{SG}, R_{in} and R_{polar} for a **ZE_SG** sample calculated after the fitting. In the beginning of the test the main contribution to the impedance of the system is due to R_{in} with a value of ~2.7×10^9 ohm cm^2. The resistance of the sol–gel falls from 2.3×10^7 on the 1st hour, to 7×10^5 ohm cm^2 after 5 days of immersion and is likely associated with electrolyte uptake and enlargement of sol–gel pores due to corrosion. On the 3rd day of immersion R_{polar} becomes prevalent in the system impedance. Visually, after this time, tiny gas bubbles (hydrogen) appeared at the sample/electrolyte interface pointing to the destruction of the coating and to corrosion onset. On the 7th day about 50% of the coating was exfoliated from the surface (Fig. 5a) and the test was stopped. Although the sol–gel coating alone provides high initial values of system impedance, its protective properties, adhesion and interface stability are insufficient for magnesium – corrosion starts after 3 days of exposure to 3% NaCl. This can be related with the fact that these types of sol–gel coatings are easily decomposed in highly alkaline environments, characteristic for Mg corrosion. As soon as local corrosion of Mg starts, hydroxyl ions, generated at an exponential rate, are consumed for alkaline hydrolysis of the silanes in the sol–gel coating.

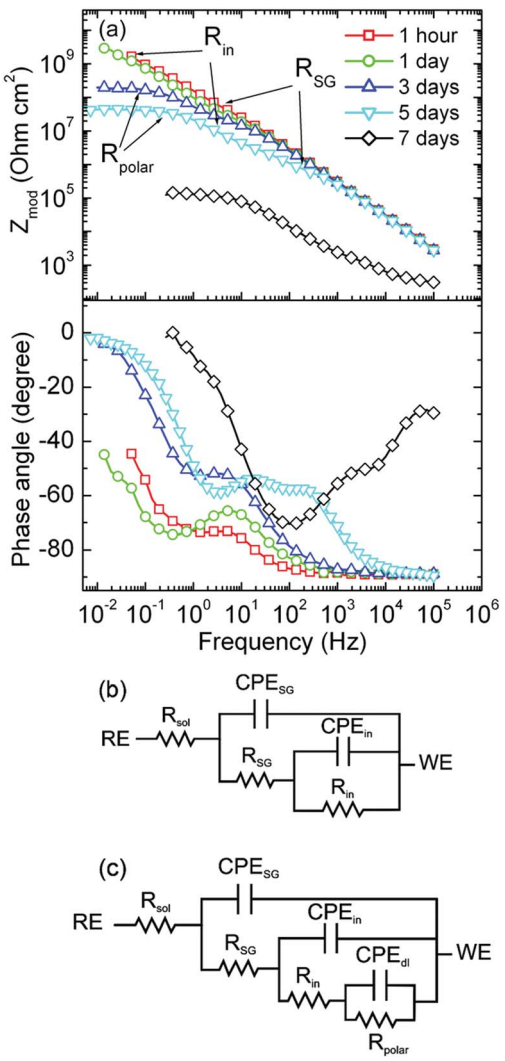

Fig. 3 Evolution of Bode plots for **ZE_SG** sample in 3% NaCl (a) and equivalent circuits used for fitting experimental EIS spectra at different immersion times (b and c).

3.3. Protective behavior of composite coatings

The total thickness of the protective coating varied between 7.8 to 8.4 μm with only the PEO layer being enriched with corrosion inhibitor. The evolution the EIS response from **ZE_Anod_SG** and **ZE_Anod_Tr_SG** specimens during immersion test is

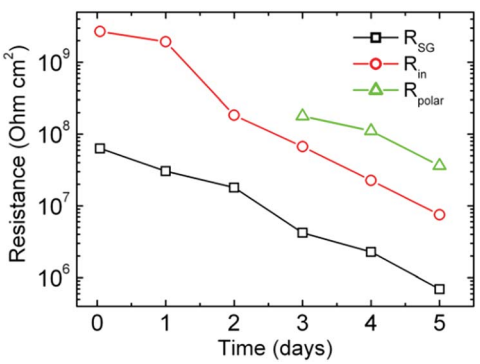

Fig. 4 Evolution of R_{SG}, R_{in} and R_{polar} for **ZE_SG** sample over the course of immersion in 3% NaCl solution.

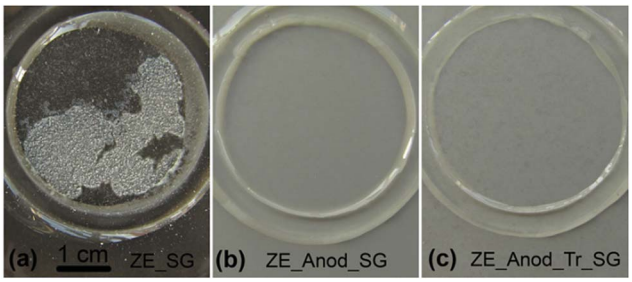

Fig. 5 Optical photographs of **ZE_SG** after 7 days (a) and **ZE_Anod_SG** (b), **ZE_Anod_Tr_SG** (c) samples after 30 days of immersion in 3% NaCl solution. The area exposed to the immersion test is 3.3 cm^2.

shown in Fig. 6. After 1 hour of immersion, the phase shift approaching $-90°$ over the wide interval of frequencies and high values of $|Z|$ ($\sim 10^{9/10}$ ohm cm^2) at low frequencies, is indicative for a compact barrier coating on both samples. After 30 day of continuous exposure to 3% NaCl solution the low frequency values of $|Z|$ drop to 3×10^8 and 4×10^8 ohm cm^2 for **ZE_Anod_SG** and **ZE_Anod_Tr_SG** samples correspondingly.

Although the low frequency impedance decreased by 1.5 orders of magnitude over one month of exposure to 3% NaCl, the impedance values remain high and no evidence of corrosion attack was observed. This can be ranked as good protective behavior, especially given the thickness of the coating being only *ca.* 8 μm.

To get a deeper insight into the behaviour of complex protective coatings, the EIS spectra were simulated and fitted. At early stages of the test the EIS spectra of both samples could be adequately fitted using a model with two time constants connected in cascade (Fig. 6b). After the 3rd day of the test the equivalent circuit with three CPE (Fig. 6c) makes physical sense and better fits the spectra. The elements R_{SG} and CPE_{SG} are attributed to the sol–gel film, R_{mix} and CPE_{mix} are resulting from the porous anodic layer with sol–gel. R_{ox} and CPE_{ox} are related to the inner dense oxide layer. The latter parameters could serve as indicators for resistibility of the complex coating towards corrosion attack since the dense oxide layer is the last barrier between magnesium corrosive media.

Fig. 7 depicts the evolution of R and capacitance values over the course of the test. In general, both inhibitor doped and undoped systems show nearly the same dynamics in the parameters of the electrical circuit. At the beginning of the test the resistance response mainly originates from the intermediate oxide–SG layer (R_{mix}) (Fig. 7a). The rapid drop of the values of R_{SG} and R_{mix} is observed during the initial 3 days and could be associated with electrolyte uptake.[24,39] At time periods of more than 7 days a slight increase for R_{mix} is observed and is

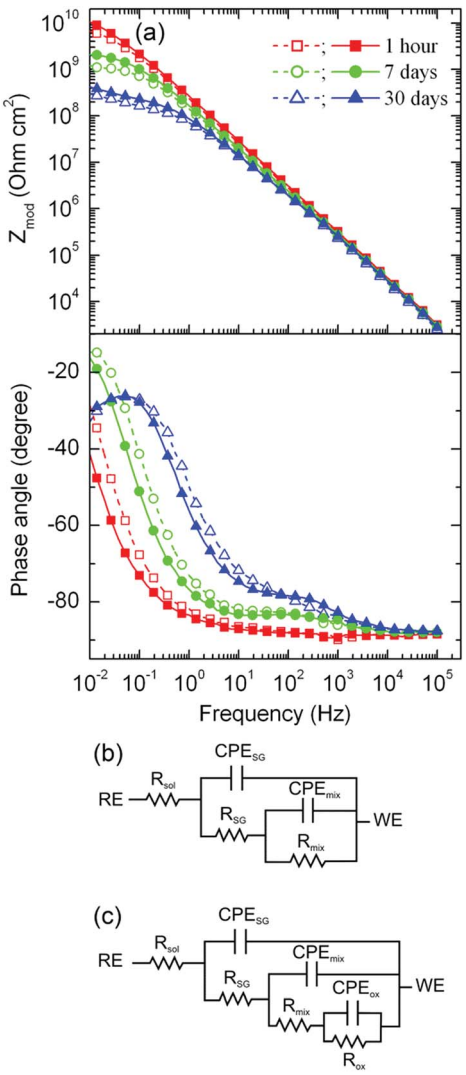

Fig. 6 Evolution of Bode plots (a) for **ZE_Anod_SG** (dashed lines, hollow marks) and **ZE_Anod_Tr_SG** (solid lines, filled marks) samples in 3% NaCl; equivalent circuits used for fitting experimental EIS spectra at different immersion times (b and c).

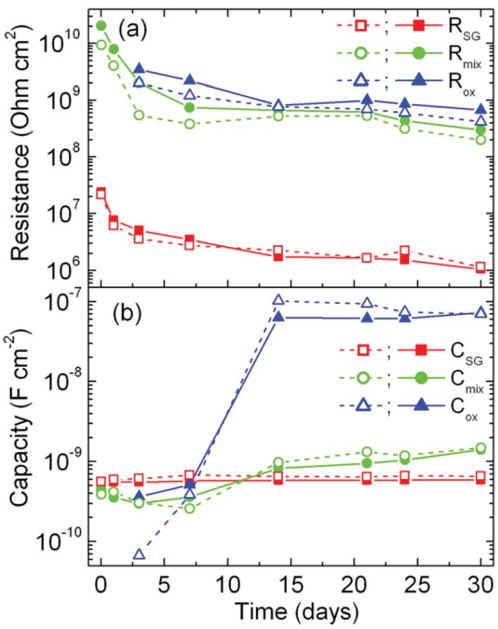

Fig. 7 Equivalent circuit parameters: resistance (a) and capacity (b) *vs.* time of immersion in 3% NaCl for **ZE_Anod_SG** (dashed lines, hollow marks) and **ZE_Anod_Tr_SG** (solid lines, filled marks).

more pronounced for the **ZE_Anod_SG** sample. This behaviour could be due to formation of magnesium hydroxide from magnesium oxide. Hydroxide seals and densifies cracks and pores the anodized layer.[24]

After the 3rd day, when the sol–gel film and mixed oxide–SG layer is already penetrated by electrolyte, the resistance of the dense barrier layer is prevalent in both systems. At the 30st day of the test the parameter R_{ox} has a rather high value for both samples: 4×10^8 ohm cm^2 for **ZE_Anod_SG** and 7×10^8 ohm cm^2 for **ZE_Anod_Tr_SG**.

The sol–gel capacitance (Fig. 7b) changes slightly with time and remains nearly constant over the course of the test, indicating the stability of the outer protective layer. CPE_{ox} is the parameter that undergoes the most noticeable changes. The rapid increase of the capacitance CPE_{ox} between 3 to 7 days could be associated with electrolyte penetration into the coating, thus facilitating a better response from the capacitor which is formed by the dense oxide layer at the metal/coating interface. It is noteworthy that after 7 days the CPE_{ox} values practically do not change, showing good protection of the inner barrier layer.

Neither the EIS data points at corrosion onset nor optical images (Fig. 5b and c). No pits, defects, crevices or filiform corrosion were observed after 30 days of exposure. Similar EIS behaviour points to the important fact that the inhibitor loaded into the porous PEO layer has no negative affect on the sol–gel upper coating. This means that both systems perform well and provide virtually the same level of corrosion protection under constant conditions. This is predictable since the corrosion processes are not yet visible in impedance spectra as the main action of the embedded inhibitor is expected on the onset of corrosion. This also leads to the important conclusion that a porous PEO layer can be used successfully as a reservoir for corrosion inhibitors while also possessing the property of an additional barrier layer. This might be especially attractive given the fact that multiple particle- and capsule-like containers reported to be used for loading corrosion inhibitors in sol–gel and other coatings[48–50] are costly and their use is associated with multiple challenges on an industrial scale, like agglomeration, dispersion in the coating, compatibility with coating matrix, *etc.*

During the real service-life of a coating defects, cracks, abrasions, *etc.* usually appear. The SVET was used to study the performance of both complex coatings in conditions simulating coating damage.

SVET allows non-invasive measurements of localized corrosion currents in micro-defects during immersion tests. For SVET measurements 0.05 M NaCl solution was used. Coated surfaces of Mg alloy AZ31 were reported to be analyzed by SVET at artificial needle-defect zones.[44,51] SVET was also used for quantitative evaluation of "self-healing" effects of corrosion inhibitor when it is distributed in protective coating deposited on a metal surface.[52] Artificial defects simulate the coating

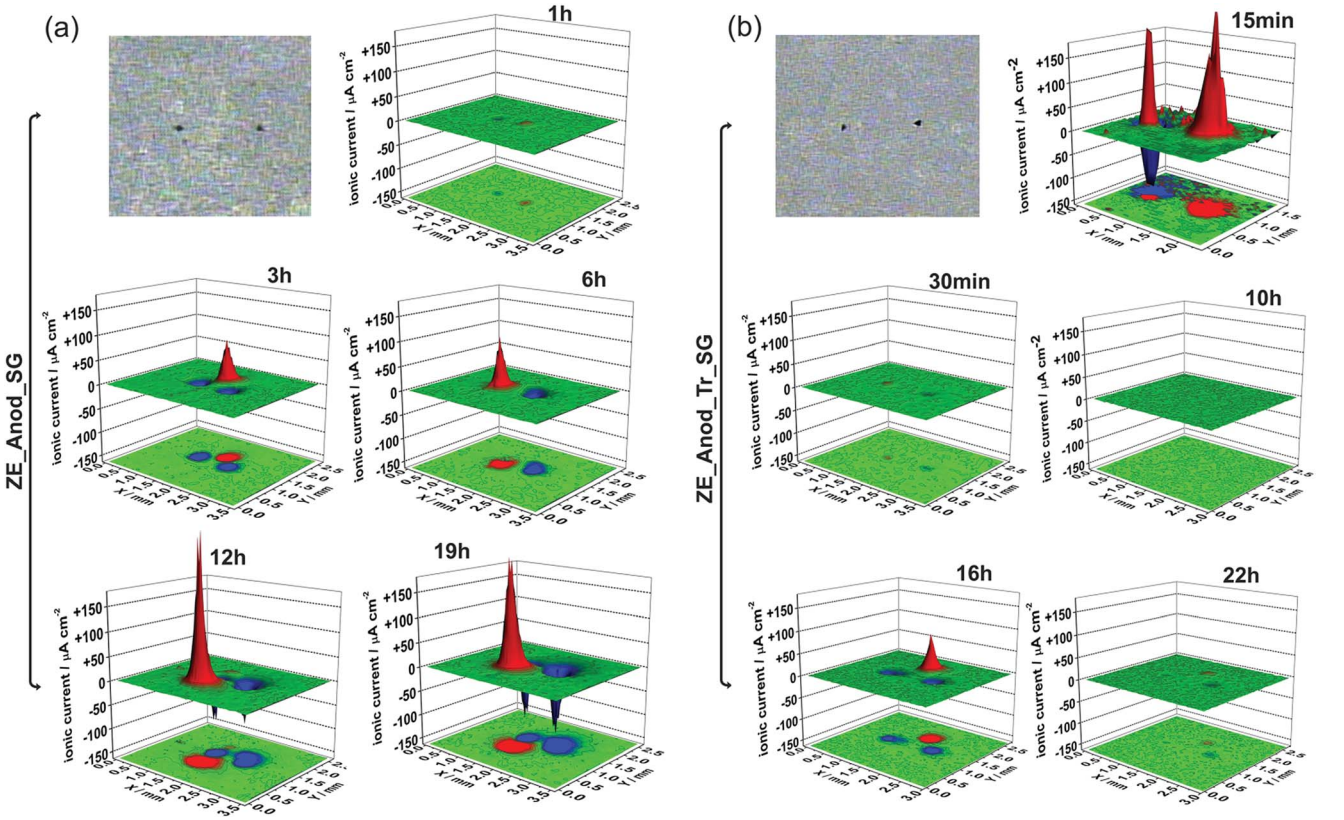

Fig. 8 Microphotographs of scanned area and distribution of ionic currents for **ZE_Anod_SG** (a) and **ZE_Anod_Tr_SG** (b) after different immersion times in 0.05 M NaCl solution. The size of the scanned area shown in optical micrograph is 2.7 × 3.7 mm.

damage as might occur during its service-life. In this study two defects (with the diameter of 200 μm each) were created in the coating using a hard needle.

SVET maps with optical photographs are presented in Fig. 8. For the **ZE_Anod_SG** sample a noticeable ionic current, associated with corrosion process, appeared after only 3 hours of immersion when an anodic and cathodic current of ~50 μA cm^{-2} were detected (Fig. 8a (3 h)).

Interesting is that, at this time, the anodic activity has already moved from the initial defect to another location evidencing initiation of an active and very mobile zone of filiform corrosion attack beneath the coating. At later times of 6, 12 and 19 h, cathodic and anodic currents from under the coating gradually increased (Fig. 8a).

The sample enriched with corrosion inhibitor, **ZE_Anod_Tr_SG**, showed distinctly different behaviour. Intensive corrosion attack was detected at the very beginning of the test after the first 15 minutes of immersion in 50 mM NaCl, (Fig. 8b (15 min)). However, after 30 min of exposure this strong activity was suppressed by the inhibitor to negligible values, clearly showing a "self-healing" effect of this composite coating. The bare Mg surface in the defect remained unaffected by corrosion attack within the next 10 hours (Fig. 8 (10 h)). The filiform corrosion near the artificial defect on **ZE_Anod_Tr_SG** occurred only at the 16^{th} hour of exposure, that is a 5 times better result compared to the coating with no inhibitor. Moreover, the filiform corrosion attack was also suppressed by the inhibitor after 16 hours of exposure and nearly eliminated by 22 hour of immersion (Fig. 8b (22 h)).

It is clearly seen that the corrosion activity on the undoped sample is gradually increases during the period of the test. An active and long-lasting mechanism against corrosion attack ("self-healing") is observed for the **ZE_Anod_Tr_SG** sample at 30 min and 16 hours of immersion and manifests itself in a sharp decrease of ionic current. The rate of corrosion for an inhibitor-doped coating is 3 to 100 times lower compared to the undoped coating throughout the entire immersion period of 24 hours. This result is in agreement with data reported by K. Fukumura and O. V. Karavai, where 1,2,4-triazole was described as inhibitor that reduced corrosion attack of Mg thought sol–gel coatings.[43,44] The designed in this work self-healing composite coating might be utilized for active protection of magnesium components that are exposed to both aggressive media and (or) mechanical impact. Formation of thin PEO coating (1.8 μm) is considerably less energy consuming than growing traditional thick PEO (>20 μm). Meanwhile even thick PEO layers need extra sealing for applications where corrosion resistance is important. Our approach consists in imparting the property of active corrosion protection to the coating by homogeneously enriching thin porous PEO layer with corrosion inhibitor. Its leaching is moderated by the thin sol–gel coating which also improves corrosion protection and assures good compatibility of PEO with the top paint.

4. Conclusions

The active corrosion protection coatings composed of a PEO layer enriched with corrosion inhibitor 1,2,4-triazole and sealed with a novel, silica based, TiO_2 doped sol–gel coating were applied to magnesium alloy ZE41. The thickness of the PEO layer is 1.8 μm and the thickness of the sol–gel film is 6.3 μm. The novel sol–gel film possessed high barrier properties at relatively low thickness. Sealing the PEO layer with the sol–gel film significantly improved protection of ZE41 from corrosion. For the sealed samples the low frequency impedance modules resulted in values higher than 10^8 ohm cm^2 after 30 days of immersion in aggressive 3% NaCl. No signs of corrosion onset were observed. The porous PEO oxide/hydroxide acted as an effective repository for 1,2,4-triazole: neither the inhibitor released into the sol–gel film at the stage of application nor the presence of 1,2,4-triazole in the PEO layer impairs the protective properties of the composite coating under constant conditions. Localized SVET measurements on artificially formed defects showed the active corrosion protection effect for the composite coating loaded with 1,2,4-triazole. Corrosion attack was reduced by a factor of 3 to 100 in the course of immersion in 50 mM solution of NaCl.

In such composite self-healing coatings, the thin porous PEO layer apart from providing barrier protection can also be successfully used as a reservoir for corrosion inhibitors. In this case, the inhibitor is secured at close proximity to the bulk metal where corrosion starts and its leaching is moderated by the thin, sol–gel coating on top of the PEO layer.

Acknowledgements

Portuguese Foundation for Science and Technology (FCT), project Fatomag, PTDC/CTM-MET/112831/2009. The financial support of FCT in frame of REDE/1509/RME/2005 project is gratefully acknowledged. K. A. Yasakau thanks FCT for Post-Doctoral grant (ref. SFRH/BPD/80754/2011). Airbus Group Innovations, Munich, Germany for supplying the alloys. S. Kallip thanks FCT for grant IF/00856/2013. S. V. Lamaka thanks the Alexander von Humboldt foundation for financial support of her Experienced Researcher grant.

Notes and references

1 G.-L. Song, *Corrosion Prevention of Magnesium Alloys*, A volume in Woodhead Publishing Series in Metals and Surface Engineering, 2013, p. 3.
2 R. C. Zeng, J. Zhang, W. Huang, W. Dietzel, K. U. Kainer, C. Blawert and W. Ke, *Trans. Nonferrous Met. Soc. China*, 2006, **16**, 763.
3 S. Abela, Protective Coatings for Magnesium Alloys, in *Magnesium Alloys – Corrosion and Surface Treatments*, ed. F. Czerwinski, InTech, Rijeka, 2011, p. 195.
4 J. E. Gray and B. Luan, *J. Alloys Compd.*, 2002, **336**, 88.
5 J. Zhang and C. Wu, *Recent Pat. Corros. Sci.*, 2010, **2**, 55.
6 R.-G. Hu, S. Zhang, J.-F. Bu, C.-J. Lin and G.-L. Song, *Prog. Org. Coat.*, 2012, **73**, 129.
7 R.-C. Zeng, F. Zhang, Z.-D. Lan, H.-Z. Cui and E.-H. Han, *Corros. Sci.*, 2014, **88**, 452.

8 J. M. Hernández-López, A. Němcová, X. L. Zhong, H. Liu, M. A. Arenas, S. J. Haigh, M. G. Burke, P. Skeldon and G. E. Thompson, *Electrochim. Acta*, 2014, **138**, 124.
9 H. Fukada and Y. Matsumoto, *Corros. Sci.*, 2004, **46**, 2135.
10 J. Yahalom and O. Khaselev, *J. Electrochem. Soc.*, 1998, **145**, 190.
11 M. Santamaria, F. Di Quarto, S. Zanna and P. Marcus, *Electrochim. Acta*, 2011, **56**, 10533.
12 C. Blawert, W. Dietzel, E. Ghali and G. Song, *Adv. Eng. Mater.*, 2006, **8**(6), 511.
13 R. Arrabal, E. Matykina, T. Hashimoto, P. Skeldon and G. E. Thompson, *Surf. Coat. Technol.*, 2009, **203**, 2207.
14 Y. Choi, S. Salman, K. Kuroda and M. Okido, *Corros. Sci.*, 2012, **63**, 5.
15 L. Chai, X. Yu, Z. Yang, Y. Wang and M. Okido, *Corros. Sci.*, 2008, **50**, 3274.
16 J. T. S. Lim, H. S. Ryu and S.-H. Hong, *Corros. Sci.*, 2012, **62**, 104.
17 P. Bala Srinivasan, J. Liang, R. G. Balajeee, C. Blawert, M. Störmer and W. Dietzel, *Appl. Surf. Sci.*, 2010, **256**, 3928.
18 A. L. Yerokhin, A. Shatrov, V. Samsonov, P. Shashkov, A. Leyland and A. Matthews, *Surf. Coat. Technol.*, 2004, **182**, 78.
19 A. S. Shatrov, Pat. WO 1999031303 A8, 2001.
20 D. E. Bartak, B. E. Lemieux and E. R. Woolsey, *US Pat.*, 5240589A, 1993.
21 E. L. Schmeling, B. Roschenbleck and M. H. Weidemann, *US Pat.*, 4978432, 1990.
22 T. F. Barton, J. A. Macculloch and P. N. Ross, *US Pat.*, 6280598 B1, 2001.
23 P. Shi, W. F. Ng, M. H. Wong and F. T. Cheng, *J. Alloys Compd.*, 2009, **469**, 286.
24 S. V. Lamaka, G. Knornschild, D. V. Snihirova, M. G. Taryba, M. L. Zheludkevich and M. G. S. Ferreira, *Electrochim. Acta*, 2009, **55**, 131.
25 U. Malayoglu, K. C. Tekin and S. Shrestha, *Surf. Coat. Technol.*, 2010, **205**, 1793.
26 Z. Li, X. Jing, Y. Yuan and M. Zhang, *Corros. Sci.*, 2012, **63**, 358.
27 D. K. Ivanou, M. Starykevich, A. D. Lisenkov, M. L. Zheludkevich, H. B. Xue, S. V. Lamaka and M. G. S. Ferreira, *Corros. Sci.*, 2013, **73**, 300.
28 R. Arrabal, J. M. Mota, A. Criado, A. Pardo, M. Mohedano and E. Matykina, *Surf. Coat. Technol.*, 2012, **206**, 4692.
29 S. V. Gnedenkov, S. L. Sinebryukhov, D. V. Mashtalyar, I. M. Imshinetskiy, A. S. Gnedenkov, A. V. Samokhin and Y. V. Tsvetkov, *Vacuum*, 2015, **120**, 107.
30 X. Guo, K. Du, Q. Guo, Y. Wang and F. Wang, *Corros. Sci.*, 2012, **65**, 367.
31 L. Zeng, S. Yang, W. Zhang, Y. Guo and C. Yan, *Electrochim. Acta*, 2010, **55**, 3376.
32 G.-L. Song, *Surf. Coat. Technol.*, 2009, **203**, 3618.
33 F. Liu, J. Yu, Y. Song, D. Shan and E.-H. Han, *Mater. Chem. Phys.*, 2015, **162**, 452.
34 C. J. Brinker and G. Scherrer, *Sol–Gel Science: the Physics and Chemistry of Sol–Gel processing*, Academic Press, San Diego, CA, 1990.
35 J. Wen and G. L. Wilkes, *Chem. Mater.*, 1996, **81**, 667.
36 D. Wang and G. P. Bierwagen, *Prog. Org. Coat.*, 2009, **64**, 327.
37 A. Khramov, V. Balbyshev, L. Kasten and R. Mantz, *Thin Solid Films*, 2006, **514**, 174.
38 M. Montemor and M. Ferreira, *Electrochim. Acta*, 2007, **52**, 7486.
39 F. Brusciotti, D. V. Snihirova, H. Xue, M. F. Montemor, S. V. Lamaka and M. G. S. Ferreira, *Corros. Sci.*, 2013, **67**, 82.
40 M. Zaharescu, L. Predoana, A. Barau, D. Raps, F. Gammel, N. C. Rosero-Navarro, Y. Castro, A. Duran and M. Aparicio, *Corros. Sci.*, 2009, **51**, 1998.
41 A. F. Galio, S. V. Lamaka, M. L. Zheludkevich, L. F. P. Dick, I. L. Muller and M. G. S. Ferreira, *Surf. Coat. Technol.*, 2010, **204**, 1479.
42 Z. Shi, M. Liu and A. Atrens, *Corros. Sci.*, 2010, **52**, 579.
43 K. Fukumura, G. O. S. Kakomoto, Y. Hama, T. Hamauzu and H. Yagi, JP Pat. P2004018978, 2004.
44 O. V. Karavai, A. C. Bastos, M. L. Zheludkevich, M. G. Taryba, S. V. Lamaka and M. G. S. Ferreira, *Electrochim. Acta*, 2010, **55**, 5401.
45 S. K. Poznyak, M. L. Zheludkevich, D. Raps, F. Gammel, K. A. Yasakau and M. G. S. Ferreira, *Prog. Org. Coat.*, 2008, **62**, 226.
46 C. Scheffey, *Rev. Sci. Instrum.*, 1988, **59**, 787.
47 C. S. Hsu and F. Mansfeld, *Corrosion*, 2001, **57**, 747.
48 D. G. Shchukin, *Polym. Chem.*, 2013, **4**, 4871.
49 A. Stankiewicz, I. Szczygieł and B. Szczygieł, *J. Mater. Sci.*, 2013, **48**, 8041.
50 D. Y. Zhu, M. Z. Rong and M. Q. Zhang, *Prog. Polym. Sci.*, 2015, **49–50**, 175.
51 S. V. Lamaka, O. V. Karavai, A. A. Bastos, M. L. Zheludkevich and M. G. S. Ferreira, *Electrochem. Commun.*, 2008, **10**, 259.
52 K. A. Yasakau, S. Kallip, M. L. Zheludkevich and M. G. S. Ferreira, *Electrochim. Acta*, 2013, **112**, 236.

